EFFECT OF GEOMETRIC IMPERFECTIONS ON NONLINEAR STABILITY OF CYLINDRICAL SHELLS CONVEYING FLUID

Marco Amabili
Dipartimento di Ingegneria Industriale
Univerista di Parma
Parco Area delle Scienze 181/A
Parma, 43100 Italy
marco@me.unipr.it
Fax: +39-0521-905705

Kostas Karagiozis
Mechanical Science and Engineering Department
University of Illinois
1206 West Green Street
MEB 228, Urbana, 61820
USA
kostask@uiuc.edu

Michael P. Païdoussis
Mechanical Engineering Department
McGill University
817 Sherbrooke Street W.
Montreal,QC H3A 2K6
Canada
mary.fiorilli@mcgill.ca

Abstract

Circular cylindrical shells conveying subsonic flow are addressed in this study; they lose stability by divergence when the flow speed reaches a critical value. The divergence is strongly subcritical, becoming supercritical for larger amplitudes. Therefore the shell, if perturbed from the initial configuration, undergoes severe deformations causing failure much before the critical velocity predicted by the linear threshold. Both Donnell's nonlinear theory retaining in-plane displacements and the nonlinear Sanders-Koiter theory are used for the shell. The fluid is modelled by potential flow theory. Geometric imperfections are introduced and fully studied. Non-classical boundary conditions are used to exactly simulate the conditions of the experiments performed. Comparison of numerical and experimental results is performed.

Key words

Nonlinear, cylindrical shells, experiments, theory, imperfections, flow.

1 Introduction

Thin-walled circular cylindrical shell structures conveying fluid may be found in many engineering and biomechanical systems. There are many applications of great interest in which shells are subjected to incompressible subsonic flows. For example, thin cylindrical shells are used as thermal shields in nuclear reactors and heat shields in aircraft engines; as shell structures in jet pumps, heat exchangers and storage tanks; as thin-walled piping for aerospace vehicles. Furthermore, in biomechanics, veins, pulmonary passages and urinary systems can be modelled as shells conveying fluid.

Circular cylindrical shells containing subsonic flow are addressed in this study; they lose stability by divergence (which is a static pitchfork bifurcation of the equilibrium, exactly the same as buckling) when the flow speed reaches a critical value. According to the few available studies [see Amabili et al. (2003)], the divergence is strongly subcritical, becoming supercritical at larger amplitudes. The interaction of fluid and solid produce two or more stable solutions concurrently for specific values of the fluid flow much before the onset of the pitchfork bifurcation. However, these solutions are related to divergence in the first mode or a combination of the first and second longitudinal modes. This explains the catastrophic loss of stability for shells, with fluid flow ranging within the limit specified by the concurrent stable shell solutions, when a small perturbation is induced in the flow or on the solid surface in the form of an additional external load. This shell failure occurs at flows much smaller than the critical velocity predicted by the linear threshold because the shell 'jumps' from a stable small-amplitude solution to a severe deformation amplitude solution that coexists for the same value of the flow velocity. Thus, modern application of shells in industry must be designed with the aid of a nonlinear shell structural model to account for the subcritical behaviour of the shell, well before the linear onset of instability.

The literature on the dynamic stability of circular cylindrical shells in the presence of internal or external axial flows is quite extensive. The effects of an internal flow have been studied, for example, by Païdoussis and Denise (1972), Weaver and Unny (1973), Païdoussis (1998), Amabili and Garziera (2002a, b) and others. In the previously mentioned studies, linear shell theories and potential flow theory are used.

The studies developed in the past for the stability of circular cylindrical shells in axial flow do not agree sufficiently well with experimental results, as pointed out by Horn et al. (1974). In particular, for subsonic

Mach numbers, highly divergent and catastrophic instabilities have been encountered experimentally for clamped-clamped copper shells excited by a fully developed turbulent flow.

The problem was solved for the first time by Amabili, Pellicano and Païdoussis (1999), who discovered the post-divergence strongly subcritical behaviour. They used Donnell's nonlinear shallow-shell theory and a base of seven natural modes to study in depth the nonlinear vibrations and stability of simply supported circular cylindrical shells conveying or immersed in subsonic flow. Karagiozis et al. (2008) developed a nonlinear model for shells with clamped ends and successfully compared theoretical results with experimental data. Experiments, confirming the calculations, were performed by Karagiozis (2006) and Karagiozis et al. (2005).

For the interested reader a detailed review of linear and nonlinear studies is given in Amabili et al. (2003) and Paidoussis (2004). Further nonlinear advances are described in Amabili (2008).

In this study, a nonlinear shell theory is used because displacements larger than the shell thickness occur. However, a linear theory, namely potential flow theory, is used for the fluid. In fact, the deformation of the fluid domain is the same as for the shell, but it must be compared with the radius of the fluid domain and not with the shell thickness in order to verify if a linear model can be used. Because the shell radius is much larger than the shell thickness, a linear potential-flow model can be used in many applications. The novelties of the present study with respect to the available literature are: (i) the introduction of geometric imperfections, which give fundamental qualitative and quantitative differences with respect to a perfect shell, and their deep study; (ii) the use of more refined nonlinear shell theories retaining in-plane displacements (without the introduction of a potential stress function), i.e. the Donnell and the Sanders-Koiter theories; (iii) the introduction of non-classical boundary conditions that allows to simulate exactly the conditions used in the experiments described in Karagiozis (2006) and Karagiozis et al. (2008).

2 Fluid structure interaction for flowing fluid

This section describes the fluid and fluid-structure interaction models used in the theoretical analysis.

2.1 Fluid model

A cylindrical coordinate system x, r, θ is introduced with the origin at one shell end. The displacements of the shell middle surface are indicated with u, v, w in the axial, circumferential and radial directions, respectively; w is taken positive outward. Only radial geometric imperfections w_0 are considered and they are assumed to be associated to zero stresses, so that locked-in initial stresses are neglected. The shell has radius R, length L and thickness h. The fluid-structure interaction is described by linear potential flow theory. The shell is considered conveying incompressible flow. The fluid is assumed to be inviscid, and the flow to be isentropic and irrotational. The irrotationality property is the condition for the existence of a scalar potential function Ψ from which the velocity may be written as

$$\mathrm{v} = \nabla\Psi \tag{1}$$

The potential Ψ consists of two components: one due to the mean flow associated with the undisturbed flow velocity U in the axial direction, and the unsteady perturbation potential Φ associated with the shell motion. Thus,

$$\Psi = Ux + \Phi\,. \tag{2}$$

The components of the fluid velocities in cylindrical coordinates are given by

$$\begin{aligned} V_x &= U + \partial\Phi/\partial x\,,\\ V_\theta &= (1/r)\,\partial\Phi/\partial\theta\,,\\ V_r &= \partial\Phi/\partial r\,. \end{aligned} \tag{3}$$

The potential of the perturbation velocity satisfies the Laplace equation

$$\nabla^2\Phi = \frac{\partial^2\Phi}{\partial x^2} + \frac{\partial^2\Phi}{\partial r^2} + \frac{1}{r}\frac{\partial\Phi}{\partial r} + \frac{1}{r^2}\frac{\partial^2\Phi}{\partial\theta^2} = 0. \tag{4}$$

The perturbed pressure P may be related to the velocity potential by Bernoulli's equation for unsteady fluid flow,

$$\frac{\partial\Phi}{\partial t} + \frac{1}{2}V^2 + \frac{P}{\rho_F} = \frac{P_S}{\rho_F}\,, \tag{5}$$

where $V^2 = \nabla\Psi\cdot\nabla\Psi$, P_S is the stagnation pressure, ρ_F is the mass density of the fluid and t is time. The pressure P in the fluid domain can be written as

$$P = \bar{P} + p\,, \tag{6}$$

where $\bar{P}$ is the mean pressure and p is the perturbation pressure, assumed positive outward of the shell. For small perturbations, $V^2 = V_x^2 + V_\theta^2 + V_r^2$ can be linearized in Φ via equations (3) to $V^2 \cong U^2 + 2U\left(\partial\Phi/\partial x\right)$, and equation (5) gives the stagnation pressure $P_S = \bar{P} + \frac{1}{2}\rho_F U^2$, so that it is fixed for an assumed mean flow velocity. Then, equation (6) gives the following expression for the perturbation pressure:

$$p = -\rho_F\left(\frac{\partial\Phi}{\partial t} + U\frac{\partial\Phi}{\partial x}\right). \tag{7}$$

2.2 Boundary conditions for the shell and middle surface displacements

The following boundary conditions are imposed at the shell ends, as shown in Figure 1:

$$v = w = w_0 = 0, \qquad \text{at } x=0,\ L \tag{8a-c}$$

$$N_x = -k_a u\,, \qquad \text{at } x=0,\ L \tag{8d}$$

$$M_x = -k_r\left(\partial w/\partial x\right), \text{ at } x=0,\ L \tag{8e}$$

where N_x is the axial load per unit length, M_x is the

bending moment per unit length, k_a is stiffness per unit length of the elastic, distributed axial springs at x = 0 and L, and k_r is the stiffness per unit length of the elastic, distributed rotational springs at x=0 and L. Moreover, u, v and w must be continuous in θ.

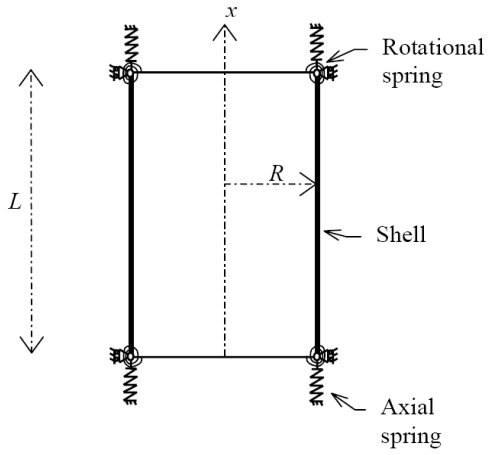

Figure 1. Scheme of studied problem.

The boundary conditions (8a,b) restrain the radial and circumferential shell displacements at both edges. Equation (8d) gives elastic axial constraint at the shell edges. Different values of the axial spring k_a are assumed for asymmetric and axisymmetric deformation modes in the numerical calculations in order to simulate experimental boundary conditions. Equation (8e) represents an elastic rotational constraint at the shell edges. It gives any rotational constraint from zero moment ($M_x = 0$, unconstrained rotation) to a perfectly rotationally clamped shell ($\partial w/\partial x = 0$, obtained as limit for $k_r \to \infty$), according to the value of k_r. For not very short thin shells, the axial springs k_a plays a much larger role than the rotational springs k_r.

A base of shell displacements is used to discretize the system; the displacements u, v and w can be expanded by using the following expressions, which identically satisfy boundary conditions (8a,b):

$$u(x,\theta,t) = \sum_{m=1}^{M_1}\sum_{j=1}^{N}\left[u_{m,j,c}(t)\cos(j\theta) + u_{m,j,s}(t)\sin(j\theta)\right] \times\cos(\lambda_m x) + \sum_{m=1}^{M_2}\cos(\lambda_m x), \quad (9a)$$

$$v(x,\theta,t) = \sum_{m=1}^{M_1}\sum_{j=1}^{N}\left[v_{m,j,c}(t)\sin(j\theta) + v_{m,j,s}(t)\cos(j\theta)\right] \times\sin(\lambda_m x), \quad (9b)$$

$$w(x,\theta,t) = \sum_{m=1}^{M_1}\sum_{j=1}^{N}\left[w_{m,j,c}(t)\cos(j\theta) + w_{m,j,s}(t)\sin(j\theta)\right] \times\sin(\lambda_m x) + \sum_{m=1}^{M_2} w_{m,0}(t)\sin(\lambda_m x), \quad (9c)$$

where j is the number of circumferential waves, m is the number of longitudinal half-waves, $\lambda_m = m\pi/L$ and t is the time; $u_{m,j}(t)$, $v_{m,j}(t)$ and $w_{m,j}(t)$ are the generalized coordinates, which are unknown functions of t; the additional subscript c or s indicates if the generalized coordinate is associated with cosine or sine function in θ, except for v, for which the notation is reversed (no additional subscript is used for axisymmetric terms). The integers N, M_1 and M_2 must be selected with care in order to obtain the required accuracy and acceptable dimension of the nonlinear problem. More terms are necessary for in-plane than for radial displacements. Torsional axisymmetric terms are not necessary since torsional axisymmetric modes are uncoupled from axial and radial axisymmetric modes. Results show a uniform convergence of the solution when adding from two to six longitudinal modes. Denoting with n the number of circumferential waves in the shape of the buckled mode, terms with j = 2n and 3n circumferential waves can be added to expansion, but they do not play an important role if geometric imperfections are not introduced.

Imperfections are expanded in the form of the following Fourier series:

$$w_0(x,\theta,t) = \sum_{m=1}^{\hat{M}}\sum_{j=0}^{\hat{N}}\left[A_{m,n}\cos(j\theta) + B_{m,n}\sin(j\theta)\right] \times\sin(m\pi x/L). \quad (10)$$

2.3 Fluid-structure interaction

When a fluid flow is considered, its behavior is not only related to what happens along the shell, but also to how the flow is constrained before and after the shell. For this reason, it is necessary to assume boundary conditions also beyond the shell. Since any system is different, and since different inflow and outflow boundary conditions do not affect the results as greatly if they are taken sufficiently away from the shell, simplified models can conveniently be introduced [see Gonçalves and Batista (1988)].

In this study, the fluid domain is assumed to be a cylinder of infinite extent, inside a periodically supported shell of infinite length, so that it is possible to employ the method of separation of variables to obtain the velocity potential. The distance between periodical supports is L. This means that the shell radial displacement w is assumed to be a periodic function with main period 2L, and the same is

satisfied by the velocity potential and perturbation pressure.

If no cavitation occurs at the fluid-shell interface, the boundary condition expressing the contact between the shell wall and the flow is

$$\left(\frac{\partial \Phi}{\partial r}\right)_{r=R} = \left(\frac{\partial w}{\partial t} + U\frac{\partial w}{\partial x}\right). \quad (11)$$

By using the method of separation of variables, Φ has the following form:

$$\Phi = \sum_{m=1}^{M}\sum_{n=0}^{N} \frac{L}{m\pi}\frac{\mathrm{I}_n\left(m\pi r/L\right)}{\mathrm{I}_n'\left(m\pi R/L\right)}\left(\frac{\partial w_{m,n}}{\partial t} + U\frac{\partial w_{m,n}}{\partial x}\right). \quad (12)$$

2.4 Energy associated with the flow

By using Green's theorem, the total energy associated with the flow is given by Amabili (2008)

$$E_{TF} = \frac{1}{2}\rho_F \iiint_{\Gamma} \mathrm{v}\cdot\mathrm{v}\,\mathrm{d}\Gamma = \frac{1}{2}\rho_F \iiint_{\Gamma} \nabla\Psi\cdot\nabla\Psi\,\mathrm{d}\Gamma$$

$$= \frac{1}{2}\rho_F \iint_{\Omega}\left(\Psi\frac{\partial\Psi}{\partial v}\right)\Bigg|_{\Omega}\mathrm{d}\Omega, \quad (13)$$

where Γ and Ω are the cylindrical fluid volume inside the shell (delimited by the length L) and the boundary surface of this volume, respectively, and v is the coordinate along the normal to the boundary, taken positive outward. Equation (13) shows that the energy E_{TF} can conveniently be divided into three terms involving different contributions of time functions and their derivatives:

$$E_{TF} = T_F + E_G - V_F. \quad (14)$$

The first and second of the three terms on the right-hand side can be identified as the kinetic and gyroscopic energies, respectively; a negative sign is used for the potential energy V_F for convenience.

2.5 Lagrange equations of motion

The following notation is introduced:

$$\mathrm{q} = \left\{u_{m,n,c}, u_{m,n,s}, v_{m,n,c}, v_{m,n,s}, w_{m,n,c}, w_{m,n,s}\right\}^{\mathrm{T}},$$

where $m = 1,...,M_1$ or M_2 and n=0,…,N. The generic element of the time-dependent vector q is referred to as q_j. The dimension of q is $\bar{N}$, which is the number of degrees of freedom (dofs) used in the mode expansion.

In the present case, the Lagrange equations of motion are rewritten as

$$\frac{\mathrm{d}}{\mathrm{d}t}\left[\frac{\partial\left(T_S + T_F\right)}{\partial\dot{q}_j}\right] - 2\frac{\partial E_G}{\partial q_j} + \frac{\partial\left(U_S + V_F\right)}{\partial q_j} = Q_j,$$

$$j = 1,\ldots,\bar{N}. \quad (15)$$

3 Experimental set-up

Experimental evidence of the nonlinear behaviour of thin metal circular cylindrical shells, supported at both ends, and subjected to internal water flow are described in the work of Karagiozis (2006) and Karagiozis et al (2005, 2008). The water-flow apparatus involves a modification of the water tunnel shown in Figure 2(a). A centrifugal pump (Ingersol-Rand Centurion S) was used to circulate water driven by an SCR-controlled 40 hp motor. The water tunnel provided average water velocities up to 6 m/s at the entrance of the plexiglas test-section, the inner diameter of which is 203 mm. Upstream of the test-section, screens and a honeycomb are used to ensure proper mixing and uniformity of the flow.

Inside the plexiglas test-section, a specially designed plastic contraction, with the shell clamped at both ends, was installed as shown in Figure 2(b, c, d). The annular space is filled with quiescent water that can be pressurized, independently of the internal pressure, via an external pressurization line. In this analysis the differential pressure (transmural pressure difference between the external averaged pressure minus the internal average pressure) is denoted by $\Delta P_{tm}(x) = P_{\mathrm{ann}} - P_{\mathrm{inn}} > 0$ for all $0 \le x \le L$, with P_{ann} being the average pressure of the annular space, not necessary related to $P_{\mathrm{inn}}(x)$ which is the internal pressure of the shell.

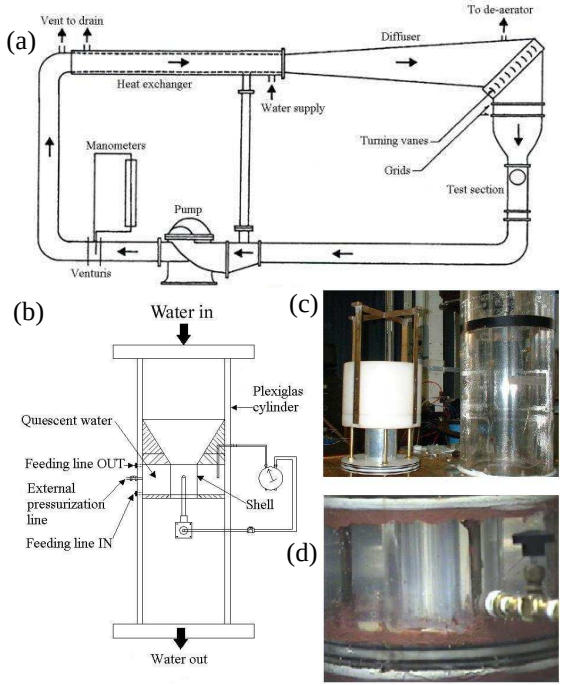

Figure 2. The water tunnel and apparatus used in the internal water-flow experiments. (a) Water tunnel set-up [after Païdoussis (1998)]; (b) the apparatus; (c) the aluminium shell mounted in the internal apparatus next to the plexiglas cylinder; (d) the shell clamped in the water tunnel apparatus.

An analog laser system (Micro-Epsilon-optoNCDT 1400-200, Daytronic 3263P) with an output of 0 to 5 Volts was used to capture the shell response throughout the experiments. Mean flow velocity measurements were made to provide information on the velocity profile inside the shell (at mid-height).

The measurements, along one diametral axis of the test-section, showed that the velocity profile is flat in the central region of the shell [see Karagiozis (2006)].

Experiments were conducted on aluminium shells glued to copper rings. The tested shells have the following dimensions and material properties: L=0.122.5 m; R=0.041125 m; h=0.000137 m; ρ_S =2720 kg/m^3, ν = 0.38 and E = 70×10^9 Pa; the radius delimiting the still fluid domain is R_1 = 0.1015 m.

A representative result of this set of experiments is shown in Figure 3. For this specific experiment the transmural pressure was set equal to $\Delta P_{tm} = P_{\text{ann}} - P_{\text{inn}} = 5.7$ kPa and it was kept constant as the flow velocity was varied; the flow velocity was increased until instability in the form of divergence occurred. The critical flow velocity was $U_c \approx 16.0$ m/s, with a circumferential wavenumber of n=6. Experimental observations indicate that the maximum amplitude of shell deformation always occurred very close to mid-length of shell; therefore, all theoretical calculations of shell amplitude were performed for $x = L/2$. In all cases the circumferential wavenumber was set equal to n=6, as observed in the experiments.

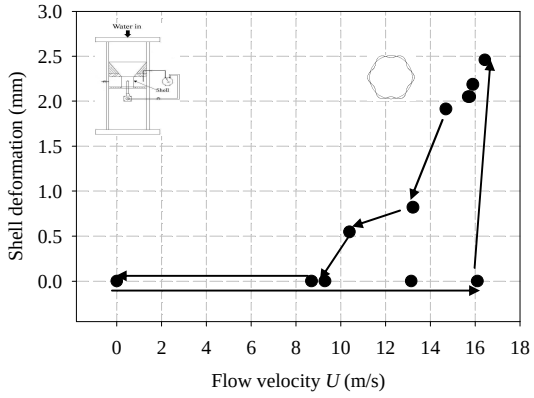

Figure 3. The shell response in a plot of the shell amplitude versus the water-flow velocity for a clamped aluminum shell with L/R=2.98 subjected to internal water-flow and inwards intramural pressurization; $\Delta P_{tm} = P_{\text{ann}} - P_{\text{inn}}(x) > 0$ and $\Delta P_{tm} = P_{\text{ann}} - P_{\text{inn}}(L/2) = 5.7$ kPa.

4 Comparison of experimental measurements and theoretical results

In all the experiments with aluminium shells, the shell lost stability by divergence, exhibiting a subcritical nonlinear postbuckling behaviour. A special note must be made about the experimental boundary conditions used in the water flow experiments. As discussed in Karagiozis et al. (2008) the experimental boundary conditions were insufficiently "good" to provide the ideal clamping of the shell assumed in theory. The copper rings used to provide the solid boundaries at the shell ends, sat on plastic supports in the test-section and were sealed with silicon rubber. This allowed for small axisymmetric motion at the interface of the shell with the bottom boundary surface of the plastic contraction, giving a boundary condition for axisymmetric modes with null axial force at the shell ends. Therefore, it is expected that the experimental results would lie between the theoretical results for simply supported and clamped-clamped shells.

In the following presentation of the numerical and experimental results, a nondimensional fluid velocity $V = U\Big/\left\{\left(\pi^2/L\right)\sqrt{D/(\rho h)}\right\}$ [see Weaver and Unny (1973)] is used, where $D = Eh^3\Big/\left[12\left(1-\nu^2\right)\right]$.

Figure 4 shows a comparison of computed and experimentally observed divergence shapes for a nondimensional flow velocity of V=2 without considering geometrical imperfections and assuming the following values for the stiffness of the axial and rotational distributed springs: $k_a = 1\times10^7$ N/m^2 and $k_r = 0.3\times10^3$ N/rad.

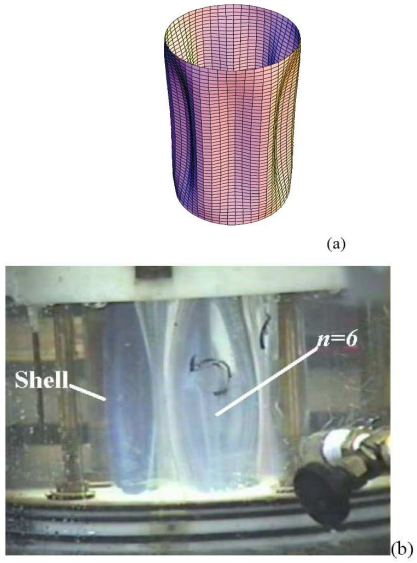

Figure 4. Comparison of computed and experimental mode shape. (a) Computed mode shape without imperfections at V=2; (b) photo of experimental divergence.

Numerical calculations showing the post-divergence behaviour of the shell for three different values of the axial and rotational distributed spring stiffness, varying from simply supported to clamped boundaries conditions, are shown in Figure 5 for a perfect shell with a model retaining 45 degrees of freedom (dofs). The results are shown in plots of the nondimensional flow velocity versus the shell deformation calculated for $x = L/2$ and a circumferential wavenumber of n=6 and transmural pressure of $\Delta P_{tm} = 5.8$ kPa. The theoretical results indicate loss of stability by divergence. Specifically, once the linear limit for the onset of instability is reached, the solution follows a subcritical line with large shell amplitudes. The unstable solution folds and become stable, as shown

in Figure 5, for all the boundary condition cases tested, ranging from simply supported to clamped-clamped ends.

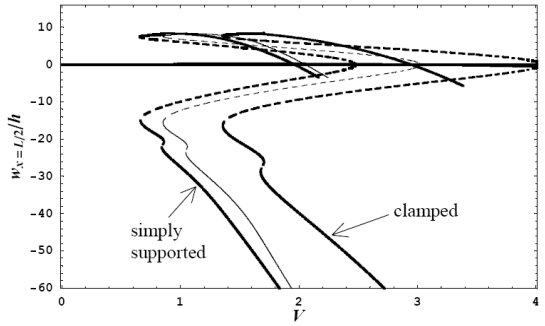

Figure 5. Effect of boundary conditions on shell divergence. ——, stable solutions; – –, unstable solutions. Thin line, $k_a = 1\times10^7$ N/m^2 and $k_r = 0.3\times10^3$ N/rad; thick line, $k_a = 0$ and $k_r = 0$ (simply supported) and $k_a = 1\times10^{11}$ N/m^2 and $k_r = 1\times10^6$ N/rad (clamped for asymmetric modes).

A comparison between theory and two experiments is shown in Figure 6.

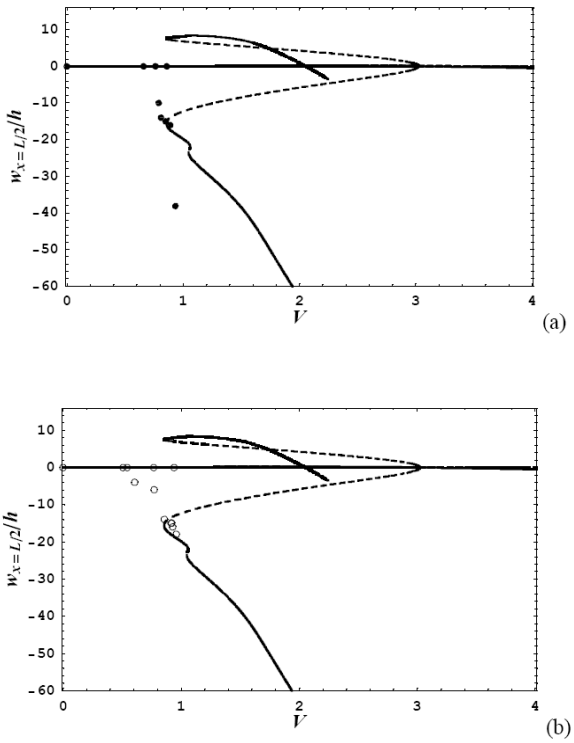

Figure 6. Comparison of numerical and experimental results. ——, stable solutions; – –, unstable solutions. Model with 45 dofs with $k_a = 1\times10^7$ N/m^2 and $k_r = 0.3\times10^3$ N/rad. (a) ●, experimental data points from the 1st set; (b) ○, experimental data points from the 2nd set.

In both theory and experiments the transmural pressure was set equal to $\Delta P_{tm} = 5.8$ kPa at x=L/2. The circumferential wavenumber used in the numerical calculations was n=6, as observed in the experiments. Qualitatively, the theoretical model is in agreement with both experiments. However, a very large difference is observed between the instability point predicted by linear theory and the actual value under perturbations, showing that a nonlinear approach is absolutely necessary for safe design of shells conveying flow.

Further improvement on the theoretical model introduced the inclusion of asymmetric imperfections, which are always present in actual shells. In this specific case the amplitude of the imperfections were set to $A_{1,n} = -3.05h$. This assumption produced an excellent agreement between numerical and experimental results, as shown in Figure 7.

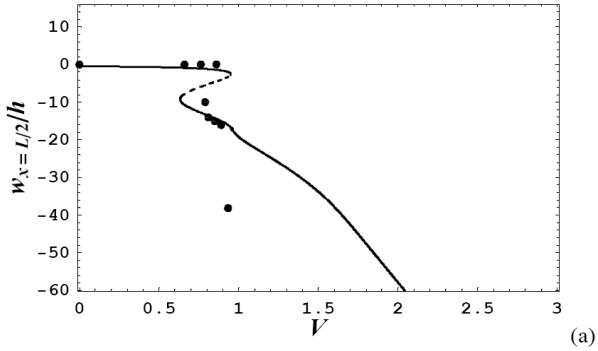

Figure 7. Comparison of numerical and experimental results for shell divergence in the case of geometric imperfections with n circumferential waves in the numerical model. Nondimensional shell amplitude at $x = L/2$ versus the nondimensional water-flow velocity for an aluminium shell with internal water flow n=6, $\Delta P_{tm}(L/2) = 5.8$ kPa, $k_a = 1\times10^7$ N/m^2 and $k_r = 0.3\times10^3$ N/rad. ——, stable solutions; – –, unstable solutions. Thin line, no imperfection; thick line, $A_{1,n} = -3.05h$. (a) ●, experimental data points from the 1st set.

5 Conclusions

Both experiments and theory are in agreement, predicting loss of stability by divergence with a strong subcritical behaviour for shells with supported ends subjected to internal subsonic fluid flow. A reasonably good quantitative agreement between experimental and theoretical results was obtained for shells with initial imperfections and mixed boundary conditions. Axisymmetric and asymmetric imperfections with a number of circumferential waves which is not a multiple of number of waves at instability play a small role. Calculations show the convergence of the solution and the accuracy of Donnell's theory retaining in-plane displacements for thin shells.

Linear analysis cannot predict the subcritical behaviour of softening type systems investigated in this study. From the design point of view, this study shows that existing safety criteria may be inadequate to predict the behaviour of thin structures subjected to external loads, due to the subcritical bifurcation

associated with loss of stability. Thus a nonlinear analysis should be undertaken to fully explore the rich dynamics of such nonlinear coupled systems.

Acknowledgements

The authors would like to thank NSERC of Canada and FQRNT of Québec for their financial support.

References

Amabili, M. (2008). *Nonlinear Vibrations and Stability of Shells and Plates*. Cambridge University Press, New York, USA.

Amabili, M. (2003). Nonlinear vibrations of circular cylindrical shells with different boundary conditions. *AIAA Journal*, **41**, pp. 1119-1130.

Amabili, M. and Garziera, R. (2002a). Vibrations of circular cylindrical shells with nonuniform constraints, elastic bed and added mass; Part II: shells containing or immersed in axial flow. *Journal of Fluids and Structures*, **16**, pp. 31-51.

Amabili, M. And Garziera, R. (2002b). Vibrations of circular cylindrical shells with nonuniform constraints, elastic bed and added mass; Part III: shells containing or immersed in axial flow. *Journal of Fluids and Structures*, **16**, pp. 796-809.

Amabili, M. and Païdoussis, M.P. (2003). Review of studies on geometrically nonlinear vibrations and dynamics of circular cylindrical shells and panels, with and without fluid-structure interaction. *Applied Mechanics Reviews* **56**, pp. 349-381.

Amabili, M. Pellicano, F. and Païdoussis, M.P. (1999). Nonlinear dynamics and stability of circular cylindrical shells containing flowing fluid. Part I: Stability. *Journal of Sound and Vibration* **225**, pp. 655-699.

Gonçalves, P.B. and Batista, R.C. (1988). Non-linear vibration analysis of fluid-filled cylindrical shells. *Journal of Sound and Vibration* **127**, pp. 133-143.

Horn,W., Barr, G.W., Carter, L., and Stearman, R.O. (1974). Recent contributions to experiments on cylindrical shell panel flutter. *AIAA Journal* **12**, pp. 1481-1490.

Karagiozis, K.N. (2006). Experiments and theory on the nonlinear dynamics and stability of clamped shells subjected to axial fluid flow or harmonic excitation. Ph.D. Thesis, McGill University, Montreal, Canada.

Karagiozis, K.N., Païdoussis, M.P., Misra, A.K., and Grinevich, E. (2005). An experimental study of the nonlinear dynamics of cylindrical shells with clamped ends subjected to axial flow. *Journal of Fluids and Structures* **20**, pp. 801-816.

Karagiozis,K.N., Païdoussis, M.P., Amabili,M., and Misra, A.K. (2008). Nonlinear stability of cylindrical shells subjected to axial flow: Theory and experiments. *Journal of Sound and Vibration*, **309**, pp. 637-676.

Païdoussis, M.P. (1998). *Fluid-Structure Interactions: Slender Structures and Axial Flow*, Vol. 1. London: Academic Press.

Païdoussis, M.P. (2004). *Fluid-Structure Interactions: Slender Structures and Axial Flow*, Vol. 2. Elsevier Academic Press, London, UK.

Païdoussis, M.P. and Denise, J.P. (1972). Flutter of thin cylindrical shells conveying fluid. *Journal of Sound and Vibration*, **20**, pp. 9-26.

Weaver, D.S. and Unny, T.E. (1973). On the dynamic stability of fluid-conveying pipes. *Journal of Applied Mechanics*, **40**, pp. 48-52.